

## Synthesis of $\alpha$ -FeOOH nanoparticles for separation of aniline and phenol from liquid fuel: single and binary cases

Safoora Rahimi, Mansooreh Soleimani\*, Amir Reza Azadmehr

Department of Chemical Engineering, Amirkabir University of Technology (Tehran Polytechnic), No. 424, Hafez Ave, P.O. Box: 15875-4413, Tehran, Iran, Tel.: +98 21 64543152; emails: soleimanim@aut.ac.ir (M. Soleimani), Rahimi.safoora@aut.ac.ir (S. Rahimi), a\_azadmehr@aut.ac.ir (A.R. Azadmehr)

Received 16 May 2023; Accepted 30 August 2023

---

### ABSTRACT

Due to environmental concerns and operational challenges, it is necessary to remove nitrogen and oxygen-containing compounds from fuels. Adsorption is an alternative sustainable method with significant advantages. Iron oxy/hydroxides are widely used as adsorbent. This study investigates the adsorption of aniline and phenol from model liquid fuel on the  $\alpha$ -FeOOH nano-adsorbent. Synthetic goethite nanoparticles were characterized using Fourier-transform infrared spectra, X-ray diffraction, field emission scanning electron microscopy, and Brunauer–Emmett–Teller analyses. Goethite performance was studied by equilibrium and kinetic experiments in single and binary cases. Based on the kinetic experiments, the average sorption of phenol on goethite was 6%–7% slower than aniline, and the determined maximum measured adsorption capacities were 472 and 446  $\text{mg}\cdot\text{g}^{-1}$  for aniline and phenol, respectively. The sorption of these components was affected by the nature of their substituents. For both impurities, the pseudo-first-order kinetic model represents a better fit for the experimental data. The adsorption equilibrium data were defined better with the Langmuir and Sips isotherm models. Experiments suggested the chemisorption mechanism for their adsorption. According to the results, Langmuir's maximum adsorption capacities for aniline and phenol at 35°C were 369.624 and 808.21  $\text{mg}\cdot\text{g}^{-1}$ , respectively. The competitive adsorption experiments using binary aniline–phenol showed that the average selectivity was 3.13.

*Keywords:* Aniline; Phenol; Fuel purification; Adsorption; Goethite; Competitive adsorption

---

### 1. Introduction

While the worldwide energy demand is increasing continuously, petroleum provides more than 40% of this required energy. The strict environmental rules and the sensitive nature of the petroleum refining processes force the refineries and petrochemicals to eliminate undesirable impurities like sulfur, oxygen, and nitrogen-containing compounds from fossil fuels via sustainable approaches [1–3]. In addition, it is noticeable that the extracted crude oil is more contaminated over time. In other words, the amount of contaminants is increasing in recent years.

Therefore, refineries and other industries need more efficient removal methods to produce cleaner products [1,4]. Removal of nitrogen-containing compounds (NCCs) with the total concentration of 0.2%–0.3% w/w in crude oil (including basic NCCs such as pyridines, anilines and quinolines and non-basic NCCs such as indoles and carbazoles), and oxygen-containing compounds (OCCs) with the total concentration of 0.1–1% w/w, including acids, phenols, ethers, ketones, esters, furans, and lactones is necessary from different points of view [5–8]. In the abstract, NCCs must be removed due to environmental concerns [4], and OCCs should be eliminated to overcome the economic and

---

\* Corresponding author.

operational challenges of industries [1]. For more explanations, the existence of NCCs in liquid fuels, on the one hand, results in  $\text{NO}_x$  emission into the atmosphere during fuel combustion [9]. On the other hand, it limits the hydrodesulfurization process by catalyst poisoning. The tremendous amounts of OCCs in liquid fuels lead to diesel production throughout the refining process and cause severe problems like the corrosion of containers. Furthermore, it decreases the fuel quality by lowering the octane number of fuel [1].

Aniline and phenol are two aromatic compounds, including a phenyl group attached to a nitrogen-containing and an oxygen-containing group, respectively. It is reported in the literature that aromatic attached C–N and C–O bonds are much stronger than those in aliphatic rings, and their corresponding compounds are known as the most refractory ones in this category [10–12]. Therefore, removing these compounds through hydrotreating processes requires higher temperatures and more  $\text{H}_2$  consumption. Adsorptive denitrogenation (ADN) and adsorptive deoxygenation (ADO) are alternative sustainable methods with significant advantages like having easy operation conditions, low cost, flexibility, and selectivity. Therefore, adsorption is a proper method to overcome deficiencies of other conventional methods [1,2,5,13–18]. Some researchers have studied the discrete adsorption of aniline or phenol from liquid fuels using  $\text{Al}_2\text{O}_3$ , iron powders, modified mesoporous molecular sieves, activated carbon, metal–organic frameworks, hexamethylenetetramine, 1,2,4-triazole, and  $\text{AlCl}_3$  [5,7,19–22]. Nevertheless, there is no report of binary adsorption of aniline and phenol, in most cases, they exist in fuel simultaneously, and it is obligatory to assess their competitive behavior during the adsorption process. Besides the adsorption efficiency and selectivity, insolubility in fuel, physical and chemical stability, non-corrosion nature of adsorbent, and economic and environmental considerations are important factors for selecting appropriate adsorbent.

Iron oxy/hydroxides with formula  $\text{FeOOH}$  are widely used as adsorbents for gas or liquid purification [23–25]. Among these potential candidates, the “ $\alpha$ ” polymorph named goethite is well known due to its outstanding adsorption capacity over both the anionic and cationic compounds [26].

Our previous study showed that iron oxy/hydroxides could efficiently remove aniline from liquid fuel [22]. Accordingly, the present study aims to purify liquid fuel from aniline and phenol using goethite adsorbent. Iso-octane was used as the model liquid fuel during the experiments. Adsorption of aniline and phenol from liquid fuel was investigated by equilibrium and kinetic studies. Goethite selectivity over both impurities was studied through binary adsorption experiments. The probable interaction mechanisms between aniline and phenol and goethite adsorbent were presented.

## 2. Experimental

### 2.1. Materials

Analytical grades of aniline, phenol, iso-octane (anhydrous, 99%), iron(III) nitrate, and potassium hydroxide were purchased from Merck (Madrid, Spain). The chemicals were utilized as received without further purification.

### 2.2. Preparation of adsorbent

A detailed procedure of goethite synthesis was reported in our previous work [22]. It was synthesized by titration of iron(III) nitrate ( $\text{Fe}(\text{NO}_3)_3 \cdot 9\text{H}_2\text{O}$ ) solution using potassium hydroxide solution until the pH of 12. Then, the adsorbent was sonicated for 30 min, and subsequently heated at  $100^\circ\text{C}$  for 70 min. The obtained mixture was centrifuged, several times washed with deionized water and acetone, and finally dried at  $30^\circ\text{C}$  in a vacuum oven. The produced solid was crushed, and sieved to form a fine powder.

### 2.3. Adsorbent characterization

The X-ray diffraction (XRD) patterns of adsorbent were recorded using an Ital Structures MPD3000 apparatus employing  $\text{Cu K}\alpha$  radiation, with the scanning rate of 0.04/s in the  $2\theta$  range from 2 to 100. A Nicolet Nexus 670 Fourier-transform infrared (FTIR) spectrophotometer (Petaling Jaya, Selangor, Malaysia) was applied to record the FTIR patterns of adsorbent. For field emission scanning electron microscopy (FESEM) analysis, a Mira3 Tescan-XMU (Brno – Kohoutovice, Czech Republic) was used. A NOVA Series 1000-Quantachrome equipment (Recently acquired by Anton Paar QuantaTec Inc., Boynton Beach, United States of America) was used to determine the surface properties of goethite based on the Brunauer–Emmett–Teller (BET) method. Before performing BET analysis, a degassing process was performed at  $10^{-4}$  mbar and  $120^\circ\text{C}$  for 6 h.

### 2.4. Adsorption experiments

Stock solutions of aniline and phenol at the concentrations of 1,000 and 5,000  $\text{mg}\cdot\text{L}^{-1}$  were prepared, respectively, by separately dissolving them in the model liquid fuel (iso-octane). Different required concentrations of solutions were prepared by homogeneous dilution of the stock solutions with pure iso-octane. Details of aniline adsorption kinetic and equilibrium experiments have been explained in our previous work [22]. In brief, aniline kinetic experiments were performed at the concentration of 50  $\text{mg}\cdot\text{L}^{-1}$ , and equilibrium experiments were carried out at the range of 5–100  $\text{mg}\cdot\text{L}^{-1}$ .

Phenol adsorption from a solution containing 1,000  $\text{mg}\cdot\text{L}^{-1}$  phenol at room temperature and various adsorption times of 1 to 300 min was assessed to study the adsorption kinetics of phenol on goethite. To investigate the equilibrium adsorption behavior of synthesized goethite adsorbent, different phenol solutions in the concentration range of 10–3,000  $\text{mg}\cdot\text{L}^{-1}$  were used at three temperatures ( $15^\circ\text{C}$ ,  $25^\circ\text{C}$ , and  $35^\circ\text{C}$ ). The adsorption time for equilibrium experiments was determined based on kinetic studies.

The aniline/phenol selectivity was calculated by determining aniline and phenol adsorption from mixtures of aniline and phenol with the aniline/phenol concentration ratios of 1, 2, and 0.5. All the kinetic and equilibrium experiments were performed with the adsorbent/fuel ratio of 0.1  $\text{g}\cdot\text{L}^{-1}$ , with a constant agitation rate of 300 rpm and specified temperatures in an orbital shaker. After adsorption experiments, solids were separated via centrifuging of samples, and the remaining impurity concentrations in the residual solution were determined using double-beam ultraviolet-visible

spectrophotometry (Camspec, Model M350, West Yorkshire, United Kingdom) at  $\lambda_{\max}$  230 and 270 nm for aniline and phenol, respectively. The adsorption capacity of goethite for aniline, and phenol,  $q_t$ , was calculated by Eq. (1).

$$q_t = \frac{(C_0 - C_t) \times V}{m} \quad (1)$$

where  $q_t$  is the amount of adsorbate (aniline or phenol) in time  $t$  ( $\text{mg}\cdot\text{g}^{-1}$ );  $C_0$  and  $C_t$  are initial and final concentrations of the adsorbate at time  $t$  ( $\text{mg}\cdot\text{L}^{-1}$ );  $V$  is the solution volume (L), and  $m$  is the adsorbent mass (g).

Non-linear pseudo-first-order and pseudo-second-order models were utilized to investigate the kinetic measurements. The attributed equations are presented in Eqs. (2) and (3), respectively [27].

$$\frac{dq}{dt} = k_1(q_e - q) \quad (2)$$

$$\frac{dq}{dt} = k_2(q_e - q)^2 \quad (3)$$

where  $q_e$  and  $q_t$  ( $\text{mg}\cdot\text{g}^{-1}$ ) are adsorption capacity at equilibrium and time “ $t$ ”, respectively, and  $k_1$  ( $\text{min}^{-1}$ ) and  $k_2$  ( $\text{g}\cdot\text{mg}^{-1}\cdot\text{min}^{-1}$ ) are the rate constant of the pseudo-first-order and pseudo-second-order adsorption models, respectively.

Two and three-parameter non-linear isotherm models, including Langmuir [Eqs. (4) and (5)], Freundlich [Eq. (6)], Temkin [Eqs. (7) and (8)], Redlich–Peterson [Eq. (9)], Khan [Eq. (10)], and Sips [Eq. (11)] isotherm models were applied to investigate the measured equilibrium data.

$$q_e = \frac{q_{\max} K_L C_e}{1 + K_L C_e} \quad (4)$$

$$R_L = \frac{1}{1 + K_L C_0} \quad (5)$$

$$q_e = K_F C_e^{1/n} \quad (6)$$

$$q_e = \left( \frac{RT}{b} \right) \ln(K_{Te} C_e) \quad (7)$$

$$B = \frac{RT}{b} \quad (8)$$

$$q_e = \frac{AC_e}{1 + BC_e^g} \quad (9)$$

$$q_e = \frac{q_m b_k C_e}{(1 + b_k C_e)^{\alpha_k}} \quad (10)$$

$$q_e = \frac{q_s a_s C_e^{1/n}}{1 + a_s C_e^{1/n}} \quad (11)$$

where  $C_e$  ( $\text{mg}\cdot\text{L}^{-1}$ ) is the equilibrium adsorption capacity at equilibrium time, and  $q_e$  ( $\text{mg}\cdot\text{g}^{-1}$ ) is the equilibrium adsorption capacity of the adsorbent. In Eqs. (4) and (5),  $q_{\max}$  ( $\text{mg}\cdot\text{g}^{-1}$ ) is the maximum adsorbed amount of adsorbates in

the Langmuir model,  $K_L$  ( $\text{L}\cdot\text{mg}^{-1}$ ) is the Langmuir constant associated with the adsorption energy,  $C_0$  is the highest initial concentration of impurities, and  $R_L$  is the separation factor. In Eq. (6),  $K_F$  ( $\text{L}^{1/n}\cdot\text{mg}^{1-1/n}\cdot\text{g}^{-1}$ ) and  $1/n$  are Freundlich constants, attributed to the adsorption capacity and intensity of adsorption, respectively. In Eqs. (7) and (8),  $K_{Te}$  ( $\text{L}\cdot\text{g}^{-1}$ ) is the Temkin isotherm equilibrium binding constant,  $b$  is the Temkin isotherm constant,  $R$  ( $8.314 \text{ J}\cdot\text{mol}^{-1}\cdot\text{K}^{-1}$ ) is the universal gas constant,  $T$  (K) is temperature, and constant related to the heat of sorption ( $\text{J}\cdot\text{mol}^{-1}$ ). In Eq. (9),  $A$  ( $\text{L}\cdot\text{g}^{-1}$ ) and  $B$  ( $\text{L}\cdot\text{mg}^{-1}$ ) are the Redlich–Peterson constant and ‘ $g$ ’ is the Redlich–Peterson isotherm exponent.

In Eq. (10),  $q_m$  ( $\text{mg}\cdot\text{g}^{-1}$ ) and  $b_k$  ( $\text{L}\cdot\text{mg}^{-1}$ ) are constants of the Khan model, and  $a_k$  is the Khan model exponent. In Eq. (11),  $q_s$  ( $\text{mg}\cdot\text{g}^{-1}$ ) and  $a_s$  ( $\text{L}\cdot\text{mg}^{-1}$ ) are constants of the Sips model, and  $n$  is the Sips model exponent [2,22,28–33].

Each isotherm model has some assumptions, and studying them can determine the adsorption mechanism. Langmuir isotherm’s primary assumption is the occurrence of monolayer adsorption on a homogeneous surface. The maximum value for adsorption capacity, calculated by Langmuir isotherm ( $q_{\max}$ ), is one of the well-known milestones for analyzing the adsorbents performance. The separation factor ( $R_L$ ) assesses the favorability of the adsorption process when its value lies between 0 and 1. In contrast, Freundlich isotherm deliberates the heterogeneity of the adsorbent surface; thus, it returns to multilayer adsorption. Adsorption is favorable when the “ $n$ ” value is between 1 and 10. Temkin isotherm deliberates the heat of adsorption and assumes that it decreases linearly. Based on this model, the adsorption is considered a uniform distribution of binding energies. Redlich–Peterson isotherm model incorporates Langmuir and Freundlich isotherms in a single three-parameter model. Khan isotherm is a generalized model that works better for pure solutions. The calculated maximum adsorption capacity ( $q_m$ ) will be reliable at relatively high  $R$ -squared values. Sips isotherm is also a hybrid model of Langmuir and Freundlich models that represents the heterogeneous adsorption systems and evades the Freundlich model limitations of increasing the adsorbate concentration. In other words, at higher adsorbate concentrations, it predicts a monolayer adsorption capacity as Langmuir isotherm, and at lower concentrations, it converts to Freundlich isotherm [34–36].

The aniline/phenol selectivity of goethite adsorbent was calculated by Eq. (12):

$$S = \frac{q_{\text{Aniline}} / q_{\text{Phenol}}}{C_{e,\text{Aniline}} / C_{e,\text{Phenol}}} \quad (12)$$

where  $S$  is the aniline/phenol selectivity,  $q_{\text{Aniline}}$  and  $q_{\text{Phenol}}$  are adsorption capacities of the adsorbent ( $\text{mg}\cdot\text{g}^{-1}$ ) for aniline and phenol, respectively, and  $C_{e,\text{Aniline}}$  and  $C_{e,\text{Phenol}}$  are equilibrium concentrations ( $\text{mg}\cdot\text{L}^{-1}$ ) of aniline and phenol, respectively.

### 3. Result and discussion

#### 3.1. Adsorbent characterization

The FTIR spectra of goethite shown in Fig. 1 include two vast bonds at 3,406 and 3,128  $\text{cm}^{-1}$  relating to bulk

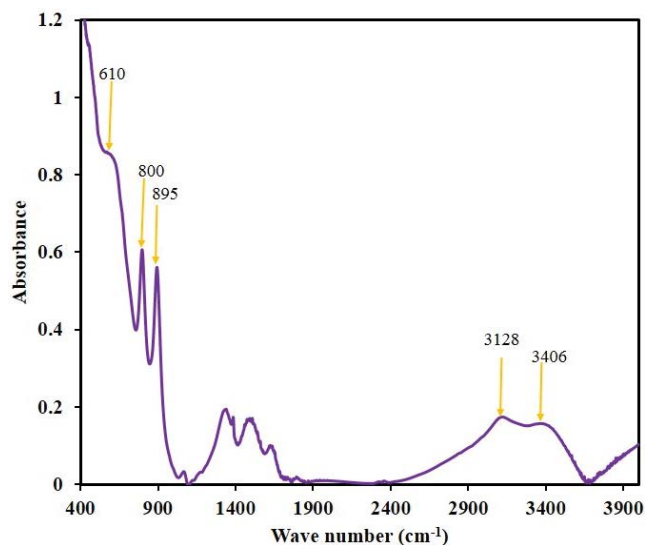


Fig. 1. Fourier-transform infrared spectra of the goethite adsorbent.

hydroxyl stretching and two O–H bending bands at 895 and 800  $\text{cm}^{-1}$  due to the in-plane and out-plane vibration of Fe–OH bond, respectively. The band appeared at 610  $\text{cm}^{-1}$ , attributes to the Fe–O stretching [33,37].

Fig. 2 shows the XRD pattern of goethite adsorbent. X'pert HighScore Plus Software (Version 3.0) and the ICDD-JCPDS database were used to analyze the results. The analysis showed that goethite has successfully been synthesized. It has an orthorhombic crystal structure with the Pbnm type space group and space group number of 62, similar to the reference pattern reported by Harrison et al. [38]. Lattice parameters determined as  $a = 4.6080 \text{ \AA}$ ,  $b = 9.9560 \text{ \AA}$ ,  $c = 3.0215 \text{ \AA}$ , and  $\alpha, \beta, \gamma = 90^\circ$ . The most intense peaks, which are at the  $2\theta$  angles of  $21.18^\circ$ ,  $33.17^\circ$ , and  $36.70^\circ$  probably are assigned to (110), (130), and (111) reflections, respectively.

Nitrogen adsorption–desorption isotherm of goethite shown in Fig. 3 indicates the type II isotherm, according to the International Union of Pure and Applied Chemistry classification with a hysteresis loop implying the combination of the microporous and mesoporous structure of adsorbent [39,40]. The porous structure results in easier access of adsorbates to active sites of adsorbent. Therefore, it could enhance the adsorption performance. According to BET results, specific surface area, total pore volume, and average pore diameter were  $128.95 \text{ m}^2\cdot\text{g}^{-1}$ ,  $169.20 \text{ mL}\cdot\text{g}^{-1}$ , and  $5.25 \text{ nm}$ , respectively.

Fig. 4 shows the FESEM images of goethite particles. These images show that the above-explained synthesis procedure has formed needle-like powders with a diameter of about 20–60 nm and a wide range of lengths (from tens to hundreds). These morphologies eventuate from hydrogen bonding and metal-oxide linkage among the octahedral chains of  $\text{Fe}^{3+}\text{O}$  [22,41,42]. As shown in Fig. 4, goethite particles tend to stick together and produce agglomerated species with different sizes in the micron-scale range. This phenomenon's main reason relates to the high coverage of hydroxyl groups on top of goethite particles' surface that causes hydrogen bonding between particles [33].

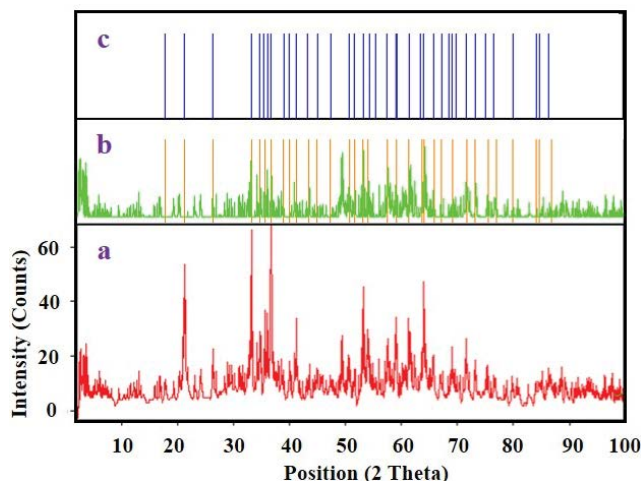


Fig. 2. X-ray diffraction pattern of goethite (a), along with its peak diagram (b) and peak diagram of the accepted reference pattern (c).

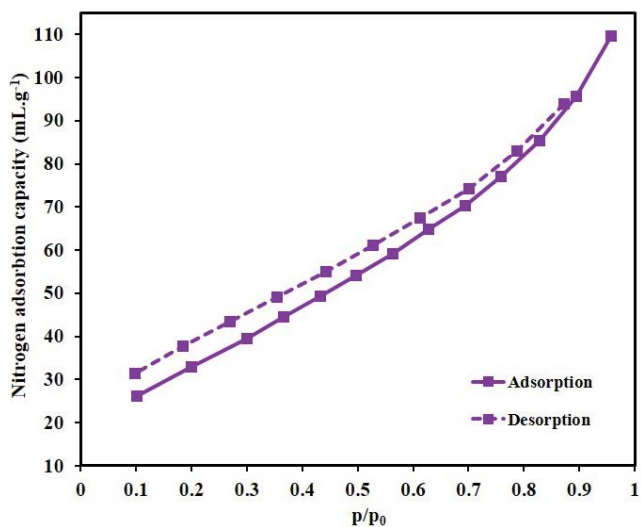


Fig. 3. Adsorption–desorption isotherms of  $\text{N}_2$  for goethite.

### 3.2. Adsorption kinetics

Kinetic measurements are illustrated in Fig. 5 using the time-capacity curves for aniline and phenol. The results revealed that at the first 20 min of the adsorption process, the adsorption capacity of aniline is 15% higher than that of phenol. It shows that aniline molecules have more tend to be adsorbed on the surface of goethite particles. It could be attributed to the more adsorption affinity of its amino substituents toward oxygen-containing functional groups of goethite. After the first 20 min, the surface saturation phenomena started, and the active adsorption sites were occupied with aniline and phenol one after another. Then, pore diffusion had been the dominant sorption route for aniline and phenol and played an important role in expediting the adsorption process. Whereas the molecular sizes of both compounds are in the same range (about 0.5–0.6 nm) [43,44], their diffusion into the adsorbent's pores does not

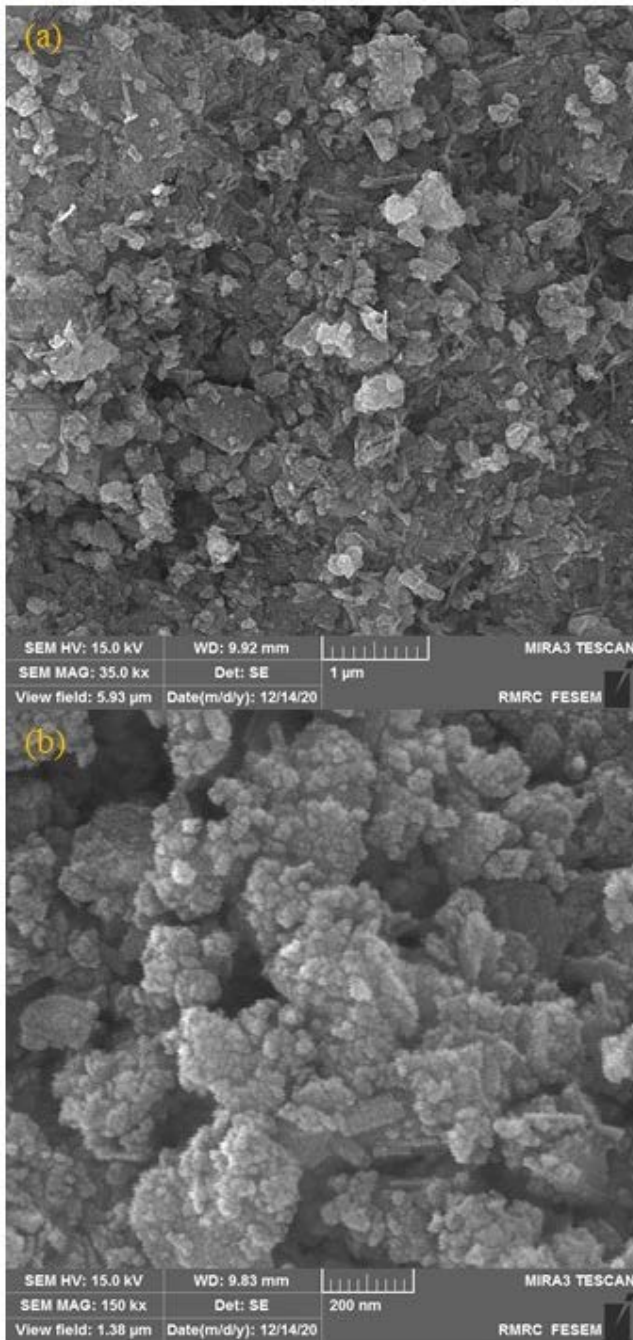


Fig. 4. Field emission scanning electron microscopy image of goethite particles with magnification of (a) 35,000x and (b) 150,000x.

make a significant difference in their pore diffusion kinetic. However, the superior interaction between aniline and adsorption sites of goethite results in slightly higher adsorption capacity values, while the initial concentration of phenol was 20 times higher than aniline. It shows that the preferable affinity of aniline onto adsorption sites of goethite makes it easier to overcome the space inhibitions caused by adsorbed similar molecules during the pore penetration process.

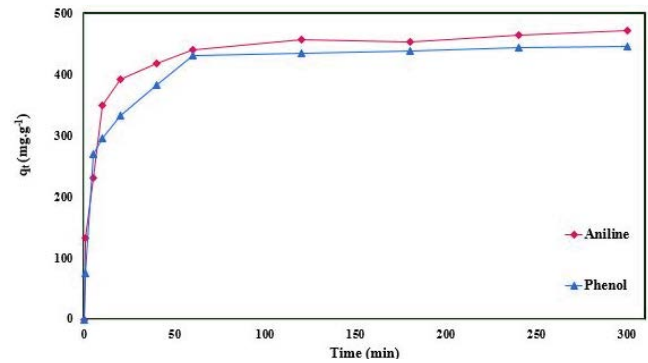


Fig. 5. Kinetic experiments of goethite adsorbents.

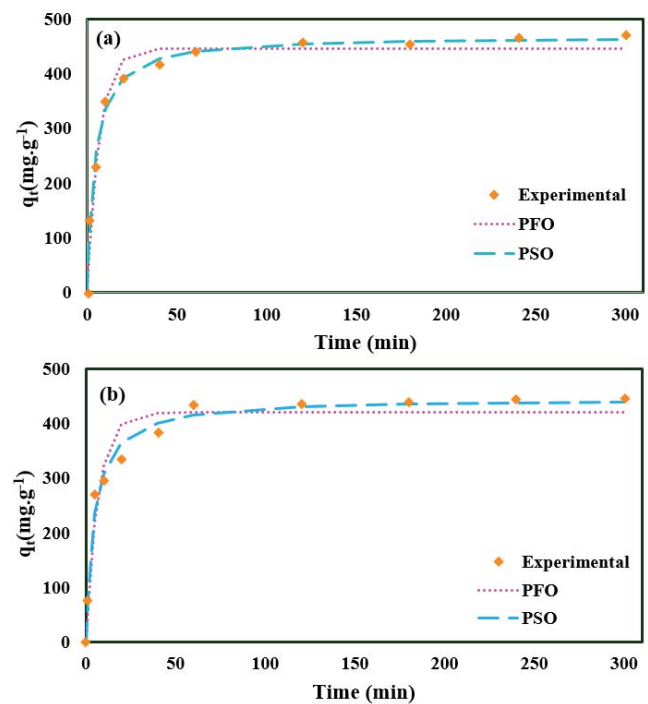


Fig. 6. Regression of pseudo-first-order and pseudo-second-order kinetic models towards the experimental kinetic data for (a) aniline and (b) phenol adsorption onto goethite.

Non-linear pseudo-first-order and pseudo-second-order kinetic models were used to describe the experimental data, and the results are presented in Fig. 6 and Table 1. As shown in Fig. 6, the observed points have more compatibility with the pseudo-second-order model. Also, comparing the  $R$ -squared values reported in Table 1 indicates that kinetic data follow the pseudo-second-order model in both cases and suggest the chemisorption adsorption mechanism. This finding confirms that chemical substituents play an important role in progressing the adsorption process.

Generally, the adsorption process contains four steps, including bulk diffusion, film diffusion, pore diffusion, and chemical interaction. The hydrophilic nature of amino and hydroxyl groups facilitates the migration of aniline and phenol from solvent bulk media and film layer towards

the oxygen-containing groups of adsorption [45]. The differences in aniline and phenol adsorption onto goethite could be due to their different substituents.

More affinity of amino groups in aniline than hydroxyl ones in phenol onto oxygen groups of adsorbent has been reported previously [46]. The amino and hydroxyl groups of adsorbates can interact with adsorbent via hydrogen bonding with surface oxide or hydroxide groups. This interaction occurs through H atoms of adsorbates with O atoms of adsorbent, and amino groups behave more reactive than hydroxyls due to their higher hydrogen content [20,47].

### 3.3. Adsorption equilibrium

Based on kinetic studies, the adsorption time for equilibrium experiments is considered to be 240 min. Fig. 7 indicates the adsorption equilibrium curves at

Table 1  
Calculated parameters of non-linear pseudo-first-order and pseudo-second-order kinetic models

Equation parameters	Impurity			
	Aniline	Phenol	Aniline	Phenol
	Pseudo-first-order kinetic model		Pseudo-second-order kinetic model	
$k$ (min <sup>-1</sup> )	0.15400	0.14639	0.00054	0.00050
$q_{e,cal}$ (mg·g <sup>-1</sup> )	446.640	420.835	469.396	446.413
R-squared	0.968	0.952	0.989	0.987

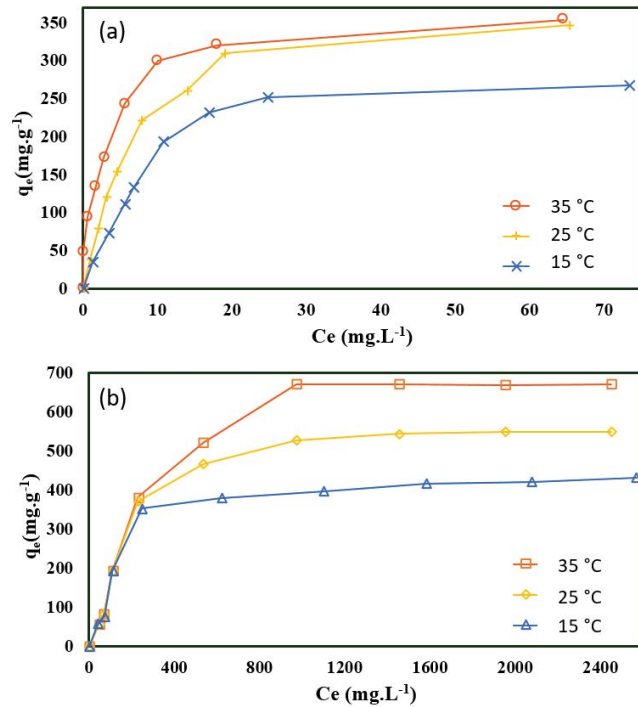


Fig. 7. Adsorption equilibrium curves at different temperatures (15°C, 25°C, and 35°C) for (a) aniline and (b) phenol onto goethite.

different temperatures of 15°C, 25°C, and 35°C for aniline and phenol onto goethite. Increasing operational temperature has a direct impact on  $q_e$ . It could be explained by the growth of mass transfer phenomena at higher temperatures that reduce the film and pore diffusion resistance between adsorbates and adsorbent.

On the other hand, it suggests a chemical mechanism for the adsorption of both purities on goethite adsorbent, as was concluded from kinetic studies. Besides, the adsorption capacities of aniline and phenol onto goethite particles were intensely enlarged by increasing their initial concentration until an optimum concentration. It happened due to more competing adsorbates occupying the adsorption sites. However, after the optimum concentration, the adsorbent would be saturated with adsorbed compounds, and increasing the initial concentration cannot improve the adsorption capacity.

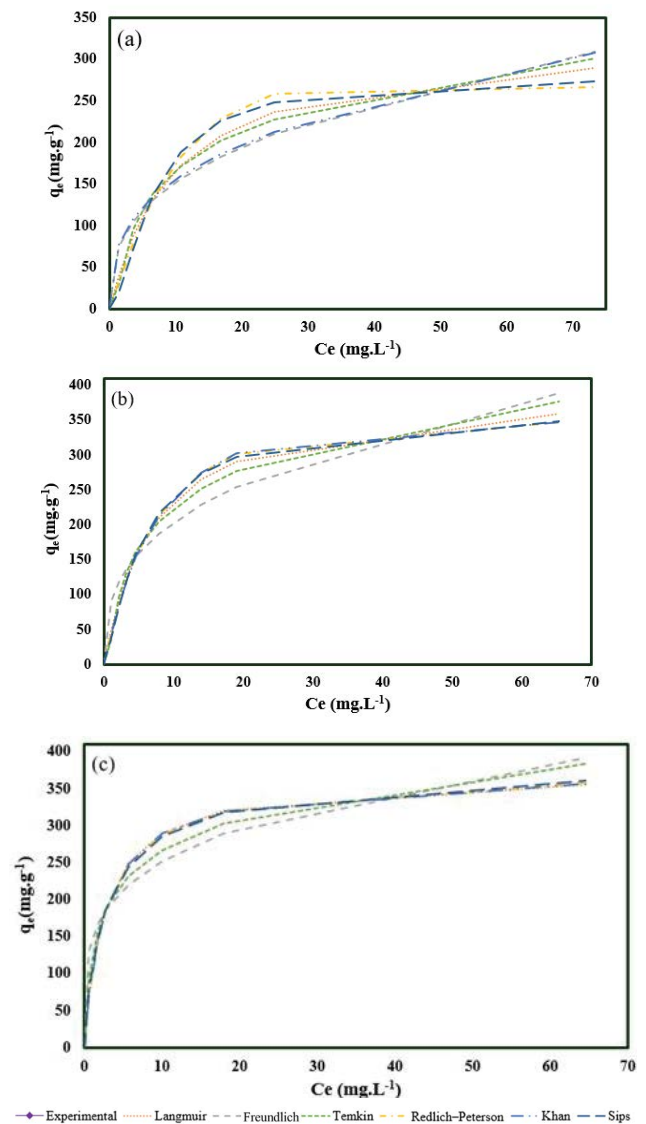


Fig. 8. Isotherm models for aniline adsorption onto goethite at (a) 15°C, (b) 25°C, and (c) 35°C.

Data are investigated by fitting them using six different isotherm models: Langmuir, Freundlich Temkin, Redlich–Peterson, Khan, and Sips isotherm models. Eqs. (4)–(11) are used to illustrate the isotherm model curvatures (Figs. 8 and 9, respectively). The values of all isotherm parameters and the model correlation coefficient are listed in Table 2. The best model can be chosen by comparing the model  $R^2$  values. Two-parameter isotherms' convenience is in the following manner:

Langmuir > Temkin > Freundlich.

It shows that the adsorption mechanism follows the monolayer coverage process. The Langmuir separation factor for all cases relies on the range of 0 to 1, confirming the adsorption process's favorability. The Sips model gives the best fit among three-parameter models. The  $n$  value in most cases is a little higher than 1, which shows the model is closer to the Langmuir model and predicts the adsorption isotherm in a nearly monolayer mechanism. These observations confirm the kinetic results of the chemisorption mechanism and agree with previously reported mechanisms [21,22,47].

### 3.4. Comparative adsorption study

Competitive experiments were performed after individual assessment of the adsorption performance of goethite

against aniline and phenol. Three different conditions were considered during competitive experiments, as shown in Table 3. Aniline/phenol selectivity of goethite was calculated using Eq. (7), and the obtained values are reported in Table 3. The results show that goethite tends to adsorb aniline more favorably than phenol, even at lower aniline concentrations. The aniline/phenol average selectivity was 3.13, which shows aniline adsorbs three times more than phenol at the same condition. This observation could be explained by more affinity of amino groups against goethite adsorbent.

## 4. Conclusion

This work studied the adsorptive performance of goethite ( $\alpha$ -FeOOH) for aniline and phenol uptake from model liquid fuel. FESEM images showed needle-like powders with an average diameter of less than 50 nm for goethite. The length of goethite particles was mainly in the range of 50–350 nm. The specific surface area of goethite was about  $129 \text{ m}^2\cdot\text{g}^{-1}$ . Experimental results showed that goethite adsorbents could effectively remove aniline and phenol from liquid fuels. The adsorption kinetic and equilibrium experiments were performed to identify the aniline adsorption mechanism and routes over synthesized goethite. It has been found that kinetic data follow the pseudo-second-order kinetic model well. Therefore, the adsorption of aniline and phenol

Table 2  
Isotherm parameters

Isotherm	Parameter	Aniline			Phenol			
		15°C	25°C	35°C	15°C	25°C	35°C	
Two-parameter isotherms	Langmuir	$q_{\max}$ ( $\text{mg}\cdot\text{g}^{-1}$ )	328.840	396.604	369.624	468.363	630.641	808.21
		$K_L$ ( $\text{L}\cdot\text{mg}^{-1}$ )	0.103	0.144	0.634	0.006	0.004	0.003
		$R_L$	0.088	0.065	0.027	0.053	0.072	0.090
		$R^2$	0.974	0.993	0.973	0.956	0.974	0.974
	Freundlich	$K_F$ ( $\text{mg}\cdot\text{g}^{-1}$ )( $\text{L}\cdot\text{g}^{-1}$ ) $^{1/n}$	67.151	91.842	14.793	46.934	42.873	40.189
		$1/n$	0.355	0.345	0.237	0.295	0.343	0.382
		$R^2$	0.870	0.903	0.922	0.865	0.888	0.889
	Temkin	$K_{Te}$ ( $\text{L}\cdot\text{g}^{-1}$ )	1.185	1.600	7.299	0.061	0.040	0.031
		$b$ ( $\text{mol}^{-1}$ )	35.574	30.629	41.178	25.742	18.508	13.613
		$B$ ( $\text{J}\cdot\text{mol}^{-1}$ )	67.309	80.891	62.186	93.018	133.487	188.104
		$R^2$	0.948	0.977	0.958	0.927	0.958	0.950
	Three-parameter isotherms	Redlich–Peterson	$A$ ( $\text{L}\cdot\text{g}^{-1}$ )	24.596	47.390	142.165	2.052	2.006
$B$ ( $\text{L}\cdot\text{mg}^{-1}$ )			0.019	0.074	0.409	0.001	0.0004	0.0001
$g$			1.334	1.119	0.983	1.230	1.259	1.410
$R^2$			0.997	0.997	0.973	0.274	0.341	0.378
Khan		$q_m$ ( $\text{mg}\cdot\text{g}^{-1}$ )	23.162	596.200	356.281	748.405	1202.97	2377
		$b_k$ ( $\text{L}\cdot\text{mg}^{-1}$ )	0.660	1.200	0.988	1.215	1.352	1.798
		$a_k$	27.139	0.083	0.387	0.003	0.002	0.001
		$R^2$	0.873	0.997	0.973	0.965	0.984	0.990
Sips		$q_s$ ( $\text{mg}\cdot\text{g}^{-1}$ )	279.920	367.065	387.203	414.824	549.098	693.170
		$a_s$ ( $\text{L}\cdot\text{mg}^{-1}$ )	0.47	0.119	0.382	0.0002	0.0001	0.0001
		$1/n$	0.631	0.822	1.161	0.446	0.560	0.602
		$R^2$	0.994	0.997	0.975	0.990	0.997	0.995

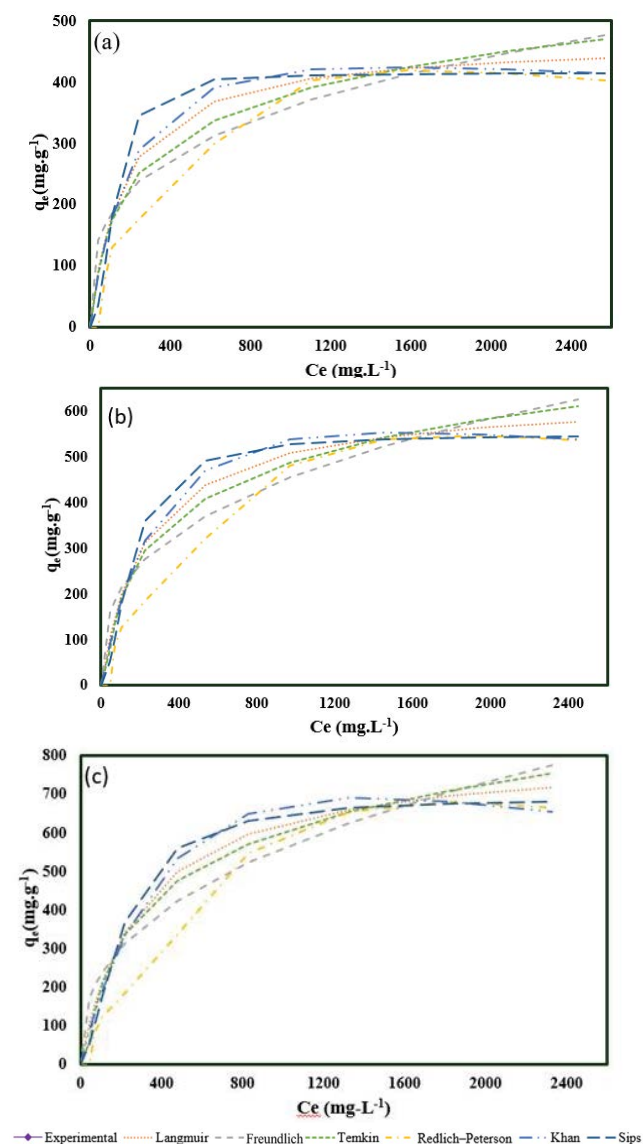


Fig. 9. Isotherm models for phenol adsorption onto goethite at (a) 15°C, (b) 25°C, and (c) 35°C.

Table 3  
Competitive experiments

Run	$C_{i,Aniline}$ (mg·L <sup>-1</sup> )	$C_{i,Phenol}$ (mg·L <sup>-1</sup> )	$S_{Aniline/phenol}$
1	100	200	2.20
2	200	100	3.13
3	200	200	4.07

onto goethite was chemisorption. The maximum adsorption capacities estimated by kinetic experiments were 472 and 446 mg·g<sup>-1</sup> for aniline and phenol, respectively. The equilibrium data were in good agreement with the Langmuir and Sips isotherm model. The Langmuir's maximum adsorption capacities for aniline and phenol at 35°C were 369.624 and 808.21 mg·g<sup>-1</sup>, respectively. The aniline/phenol average

selectivity was 3.13, which shows aniline adsorbs three times more than phenol in the same condition. The results indicated that although goethite is a strong adsorbent for phenol removal, its higher selectivity against aniline makes it a promising adsorbent for the sustainable removal of NCCs from fossil fuels.

## Funding

The authors sincerely acknowledge the National Iranian Oil Refining and Distribution Company (NIORDC), because they received financial support in the form of a research grant from this company.

## References

- [1] H.E. Emam, F.H.H. Abdellatif, R.M. Abdelhameed, Cationization of cellulose fibers in respect of liquid fuel purification, *J. Cleaner Prod.*, 178 (2018) 457–467.
- [2] M. Ahmadi, B. Anvaripour, M.R. Khosravi-nikou, M. Mohammadian, Selective denitrogenation of model fuel through iron and chromium modified microporous materials (MSU-S), *J. Environ. Chem. Eng.*, 5 (2017) 849–860.
- [3] A. Kumar, P. Muthukumar, P. Sharma, E.A. Kumar, Absorption based solid state hydrogen storage system: a review, *Sustainable Energy Technol. Assess.*, 52 (2022) 102204, doi: 10.1016/j.seta.2022.102204.
- [4] I. Ahmed, N.A. Khan, S.H. Jhung, Adsorptive denitrogenation of model fuel by functionalized UiO-66 with acidic and basic moieties, *Chem. Eng. J.*, 321 (2017) 40–47.
- [5] K. Tang, X. Hong, preparation and characterization of Co-MCM-41 and its adsorption removing basic nitrogen compounds from fluidized catalytic cracking diesel oil, *Energy Fuels*, 30 (2016) 4619–4624.
- [6] E.B. Strel'mikova, I.V. Goncharov, O.V. Serebrennikova, Concentration and distribution of oxygen-containing compounds in crude oils from the southeastern part of Western Siberia, *Pet. Chem.*, 52 (2012) 278–283.
- [7] R.M. Abdelhameed, H.E. Emam, J. Rocha, A.M.S. Silva, Cu-BTC metal-organic framework natural fabric composites for fuel purification, *Fuel Process. Technol.*, 159 (2017) 306–312.
- [8] J. Speight, Eds., *Shale Oil and Gas Production Processes*, Gulf Professional Publishing, United States, 2020, pp. 873–912.
- [9] M. Zhao, P. Xue, J. Liu, J. Liao, J. Guo, A review of removing SO<sub>2</sub> and NO<sub>x</sub> by wet scrubbing, *Sustainable Energy Technol. Assess.*, 47 (2021) 101451, doi: 10.1016/j.seta.2021.101451.
- [10] S.D. Sumbogo Murti, K.H. Choi, K. Sakanishi, O. Okuma, Y. Korai, I. Mochida, Analysis and removal of heteroatom containing species in coal liquid distillate over NiMo catalysts, *Fuel*, 84 (2005) 135–142.
- [11] M. Wang, H. Shi, D.M. Camaioni, J.A. Lercher, Palladium-catalyzed hydrolytic cleavage of aromatic C–O bonds, *Angew. Chem.*, 129 (2017) 2142–2146.
- [12] R. Prins, Catalytic hydrodenitrogenation, *Adv. Catal.*, 46 (2001) 399–464.
- [13] J. You, H. Song, J. Zhang, C. Chen, F. Han, Adsorptive removal of nitrogen-containing compounds from fuel over hierarchical porous aluminosilicates synthesized by kinetic regulation method, *Fuel*, 241 (2019) 997–1007.
- [14] M. Almarri, X. Ma, C. Song, Selective adsorption for removal of nitrogen compounds from liquid hydrocarbon streams over carbon- and alumina-based adsorbents, *Ind. Eng. Chem. Res.*, 48 (2009) 951–960.
- [15] M.S. Rana, R. Brouesli, N. Mustafa, Effect of organic nitrogen compounds on deep hydrodesulfurization of middle distillate, *Fuel Process. Technol.*, 177 (2018) 170–178.
- [16] F. López-Linares, L. Carbognani, C. Sosa Stull, P. Pereira-almao, F. Lo, L. Carbognani, C.S. Stull, P. Pereira-almao, Adsorption kinetics of anilines on macroporous kaolin, *Energy Fuels*, 22 (2008) 2188–2194.

- [17] S. Rashidi, M. Reza, K. Nikou, B. Anvaripour, Adsorptive desulfurization and denitrogenation of model fuel using HPW and NiO-HPW modified aluminosilicate mesostructures, *Microporous Mesoporous Mater.*, 211 (2015) 134–141.
- [18] L. Wang, Y. Ma, D. Xie, M. Zhang, N. Zuo, N. Mominou, C. Jing, Ultra-deep desulfurization of model diesel fuel over Pr/Ce-N-TiO<sub>2</sub> assisted by visible light, *Microporous Mesoporous Mater.*, 323 (2021) 111258, doi: 10.1016/j.micromeso.2021.111258.
- [19] S. Ardizzzone, H. Høiland, C. Lagioni, E. Sivieri, Pyridine and aniline adsorption from an apolar solvent: the role of the solid adsorbent, *J. Electroanal. Chem.*, 447 (1998) 17–23.
- [20] B.N. Bhadra, I. Ahmed, S.H. Jhung, Remarkable adsorbent for phenol removal from fuel: functionalized metal-organic framework, *Fuel*, 174 (2016) 43–48.
- [21] J. Gao, Y. Dai, W. Ma, H. Xu, C. Li, Efficient separation of phenol from oil by acid-base complexing adsorption, *Chem. Eng. J.*, 281 (2015) 749–758.
- [22] S. Rahimi, M. Soleimani, A.R. Azadmehr, Performance evaluation of synthetic goethite and lepidocrocite nano-adsorbents for the removal of aniline from a model liquid fuel through kinetic and equilibrium studies, *Energy Fuels*, 35 (2021) 10659–10668.
- [23] F. Granados-Correa, N.G. Corral-Capulin, M.T. Olguín, C.E. Acosta-León, Comparison of the Cd(II) adsorption processes between boehmite ( $\gamma$ -AlOOH) and goethite ( $\alpha$ -FeOOH), *Chem. Eng. J.*, 171 (2011) 1027–1034.
- [24] S.K. Sahoo, M. Tripathy, G. Hota, *In-situ* functionalization of GO sheets with AlOOH-FeOOH composite nanorods: an eco-friendly nanoadsorbent for removal of toxic arsenate ions from water, *J. Environ. Chem. Eng.*, 7 (2019) 103357, doi: 10.1016/j.jece.2019.103357.
- [25] G. Moradi, F. Dabirian, P. Mohammadi, L. Rajabi, M. Babaei, N. Shiri, Electrospun fumarate ferroxane/polyacrylonitrile nanocomposite nanofibers adsorbent for lead removal from aqueous solution: characterization and process optimization by response surface methodology, *Chem. Eng. Res. Des.*, 129 (2017) 182–196.
- [26] T. Yamamoto, M. Tayakout-Fayolle, C. Geantet, Gas-phase removal of hydrogen sulfide using iron oxyhydroxide at low temperature: measurement of breakthrough curve and modeling of sulfidation mechanism, *Chem. Eng. J.*, 262 (2015) 702–709.
- [27] M. Songolzadeh, M. Soleimani, M. Takht Ravanchi, Evaluation of metal type in MIL-100 structure to synthesize a selective adsorbent for the basic N-compounds removal from liquid fuels, *Microporous Mesoporous Mater.*, 274 (2019) 54–60.
- [28] H. Kargar, M. Ghahramaninezhad, M.N. Shahrak, S.S. Balula, An effective magnetic catalyst for oxidative desulfurization of model and real fuels: Fe<sub>2</sub>O<sub>3</sub>/ZIF-8/TiO<sub>2</sub>, *Microporous Mesoporous Mater.*, 317 (2021) 110992, doi: 10.1016/j.micromeso.2021.110992.
- [29] F. Chen, Q. Zhu, S. Li, Z. Xu, X. Sun, S. Zhao, The function of poly aromatic nuclei structure for adsorption of vanadyl/nickel etioporphyrin on asphaltene/graphene, *Fuel Process. Technol.*, 174 (2018) 132–141.
- [30] M. Ahmadi, M. Mohammadian, M.R. Khosravi-Nikou, Experimental, kinetic, and thermodynamic studies of adsorptive desulfurization and denitrogenation of model fuels using novel mesoporous materials, *J. Hazard. Mater.*, 374 (2019) 129–139.
- [31] D. Ursueguía, E. Díaz, S. Ordóñez, Adsorption of methane and nitrogen on basolite MOFs: equilibrium and kinetic studies, *Microporous Mesoporous Mater.*, 298 (2020) 110048, doi: 10.1016/j.micromeso.2020.110048.
- [32] S.M. Amininasab, P. Holakoei, Z. Shami, M. Hassanzadeh, Preparation and evaluation of functionalized goethite nanorods coated by molecularly imprinted polymer for selective extraction of bisphenol A in aqueous medium, *J. Polym. Res.*, 25 (2018) 1–10.
- [33] S. Rahimi, R.M. Moattari, L. Rajabi, A.A. Derakhshan, M. Keyhani, Iron oxide/hydroxide ( $\alpha,\gamma$ -FeOOH) nanoparticles as high potential adsorbents for lead removal from polluted aquatic media, *J. Ind. Eng. Chem.*, 23 (2015) 33–43.
- [34] A. Günay, E. Arslankaya, I. Tosun, Lead removal from aqueous solution by natural and pretreated clinoptilolite: adsorption equilibrium and kinetics, *J. Hazard. Mater.*, 146 (2007) 362–71.
- [35] K. State, E. State, Langmuir, Freundlich, Temkin and Dubinin-Radushkevich isotherms studies of equilibrium sorption of Zn<sup>2+</sup> onto phosphoric acid modified rice husk, *IOSR J. Appl. Chem.*, 3 (2012) 38–45.
- [36] K.Y. Foo, B.H. Hameed, Insights into the modeling of adsorption isotherm systems, *Chem. Eng. J.*, 156 (2010) 2–10.
- [37] S. Liao, J. Wang, D. Zhu, L. Ren, J. Lu, M. Geng, A. Langdon, Structure and Mn<sup>2+</sup> adsorption properties of boron-doped goethite, *Appl. Clay Sci.*, 38 (2007) 43–50.
- [38] R.K. Harrison, N. Aitkenhead, B.R. Young, P.F. Dagger, Goethite from Hindlow, Derbyshire, *Bull. Geol. Surv.*, 52 (1975) 51–54.
- [39] S. Fu, W. Han, Accurate characterization of full pore size distribution of tight sandstones by low-temperature nitrogen gas adsorption and high-pressure mercury intrusion combination method, *Energy Sci. Eng.*, 9 (2021) 80–100.
- [40] M. Songolzadeh, M. Soleimani, M.T. Ravanchi, Synthesis and optimization of a new MIL-100 adsorbent for removing basic N-compounds from liquid fuels, *Pet. Sci. Technol.*, 37 (2019) 2383–2390.
- [41] Y. Hexiong, L. Ren, R.T. Downs, G. Costin, Goethite,  $\alpha$ -FeO(OH), from single-crystal data, *Acta Crystallogr., Sect. E: Struct. Rep. Online*, 62 (2006) 250–252.
- [42] J.-P. Jolivet, C. Chanéac, E. Tronc, Iron oxide chemistry. From molecular clusters to extended solid networks, *Chem. Commun.*, 5 (2004) 481–483.
- [43] E. Lorenc-Grabowska, Effect of micropore size distribution on phenol adsorption on steam activated carbons, *Adsorption*, 22 (2016) 599–607.
- [44] J.H. Kim, T. Kim, Y.C. Jeong, K. Lee, K.T. Park, S.J. Yang, C.R. Park, Stabilization of insoluble discharge products by facile aniline modification for high performance Li-S batteries, *Adv. Energy Mater.*, 5 (2015) 1–10.
- [45] S. Yu, X. Wang, Y. Ai, X. Tan, T. Hayat, W. Hu, X. Wang, Experimental and theoretical studies on competitive adsorption of aromatic compounds on reduced graphene oxides, *J. Mater. Chem. A*, 4 (2016) 5654–5662.
- [46] D.M. Nevskaja, E. Castillejos-Lopez, A. Guerrero-Ruiz, V. Muñoz, Effects of the surface chemistry of carbon materials on the adsorption of phenol-aniline mixtures from water, *Carbon N. Y.*, 42 (2004) 653–665.
- [47] L. Jiang, L. Liu, S. Xiao, J. Chen, Preparation of a novel manganese oxide-modified diatomite and its aniline removal mechanism from solution, *Chem. Eng. J.*, 284 (2016) 609–619.